Multi-View Ensemble for Time Series Anomaly Detection via Coupling Flows

Wanghui Qiu[1,*], **Chenxi Liu**[2,*], **Shiyan Hu**[1], **Zhengyu Li**[1], **Chenjuan Guo**[1], **Bin Yang**[1,†]
[1]East China Normal University
[2]Hong Kong Institute of Science & Innovation
onehui@stu.ecnu.edu.cn, chenxi.liu@cair-cas.org.hk, syhu@stu.ecnu.edu.cn,
lizhengyu@stu.ecnu.edu.cn, cjguo@dase.ecnu.edu.cn, byang@dase.ecnu.edu.cn

Abstract

Time series anomaly detection faces a critical challenge that different anomaly types require different detection mechanisms, yet single methods are inherently limited by their design biases. We propose FlowFuse, a multi-view ensemble framework with coupling flow-based score fusion for time series anomaly detection. FlowFuse combines four complementary detection modules spanning temporal and frequency domains, as well as clustering and reconstruction paradigms, to extract multi-perspective anomaly scores. Rather than simple averaging, an ensemble of coupling flows models the joint distribution of these multi-view scores, learning complex inter-view dependencies through invertible transformations with alternating updates between temporal and frequency scores. The ensemble naturally quantifies detection uncertainty through score disagreement among ensemble members, which can optionally guide selective supervision when labels are available. Extensive experiments across 18 diverse benchmarks show that FlowFuse achieves state-of-the-art performance, demonstrating effectiveness across multiple anomaly types.

Code: https://github.com/decisionintelligence/FlowFuse

1 Introduction

Time series anomaly detection has become a critical capability across diverse real-world applications, from industrial equipment monitoring and financial fraud detection to fault diagnosis, automotive maintenance, and transportation systems [Huang *et al.*, 2022; von Birgelen and Niggemann, 2018; Guo *et al.*, 2014; Lu *et al.*, 2011; Yang *et al.*, 2023a; Ma *et al.*, 2014]. The ability to automatically identify anomalous patterns in time series data is essential for ensuring system reliability, operational safety, and service continuity [Mathur and Tippenhauer, 2016; Hundman *et al.*, 2018]. The increasing complexity and scale of modern time series data demand advanced detection methods that can capture various anomaly types effectively [Xu *et al.*, 2021; Wu *et al.*, 2022; Zamanzadeh Darban *et al.*, 2024].

Despite significant advances in anomaly detection techniques, a fundamental challenge continues to limit the performance of existing methods, that is, the inherent diversity of anomaly patterns and the inability of single detection mechanisms to handle them comprehensively [Qiu *et al.*, 2025a; Zamanzadeh Darban *et al.*, 2024]. Specifically, the first challenge stems from the diversity of time series anomaly types. Temporal anomalies manifest as either point anomalies affecting individual observations, including global and contextual anomalies [Chandola *et al.*, 2009; Lai *et al.*, 2021], or sequence anomalies spanning continuous segments, such as seasonal, trend, and shapelet anomalies [Qiu *et al.*, 2025a; Yeh *et al.*, 2016]. Researchers have developed various detection approaches, from statistical methods and classical machine learning to deep learning architectures [Breunig *et al.*, 2000; Liu *et al.*, 2008; Xu *et al.*, 2021], demonstrating excellent detection capabilities. However, different anomaly types exhibit vastly different behavioral patterns, and single detection mechanisms, constrained by their theoretical foundations and design biases, struggle to simultaneously capture these diverse characteristics (see Section 4.4). This specialization inevitably limits the applicability of individual methods in complex real-world scenarios.

The second challenge concerns how to combine multiple detection methods effectively. While ensemble approaches offer a natural solution to the diversity problem, traditional score aggregation methods, such as averaging or weighted combination, fail to capture the complex, non-linear dependencies between different detection views [Campos *et al.*, 2022]. For instance, when temporal methods detect anomalies that frequency methods correctly ignore, simple averaging dilutes the detection signal rather than leveraging the complementary information. When multiple views show moderate scores that individually seem unremarkable, their consistent deviation might indicate a true anomaly that a linear combination fails to identify [Campos *et al.*, 2022]. What is needed is a principled approach to model the *joint distribution* of multi-view scores, understanding when different views agree, disagree, or provide complementary information.

We propose FlowFuse, a framework that addresses the above challenges through principled multi-view ensemble learning with coupling flow-based score fusion. For the diversity challenge, we strategically select four complementary

detection perspectives spanning temporal vs. frequency domains, as well as clustering vs. reconstruction paradigms, extracting temporal scores and frequency scores to cover diverse anomaly types comprehensively. The coupling flow architecture learns complex dependencies among these multi-view anomaly scores through invertible transformations that alternately update temporal and frequency representations, enabling effective detection across diverse anomaly patterns. An ensemble of coupling flows further enhances robustness through model averaging while naturally quantifying detection uncertainty via score disagreement. When labeled data becomes available, this uncertainty can guide a learned router to selectively refine anomaly scores, though the framework operates effectively with a simple average router in purely unsupervised settings.

We demonstrate FlowFuse's effectiveness through extensive experiments on 10 univariate and 8 multivariate time series datasets, showing consistent superiority over 18 state-of-the-art baseline methods. FlowFuse achieves strong performance across multiple anomaly types, validating the effectiveness of principled multi-view fusion.

Our main contributions are summarized as follows:

- We propose FlowFuse, a multi-view ensemble framework that extracts complementary anomaly scores from temporal and frequency domains through four parallel detectors, and models their joint distribution using coupling flows to effectively capture different types of anomalies.
- We introduce coupling flow-based score fusion that learns complex inter-view dependencies through invertible transformations with alternating updates between temporal and frequency scores, enabling sophisticated modeling of how different detection methods complement each other beyond simple linear aggregation.
- Extensive experiments on 18 benchmarks demonstrate FlowFuse's consistent superiority over 18 state-of-the-art methods, particularly achieving strong performance across diverse anomaly types through the principled multi-view fusion approach.

2 Related Work

2.1 Anomaly Detection Paradigms

Statistical Distribution-based Methods

Statistical methods detect anomalies by finding data that differs from normal patterns [Chandola *et al.*, 2009]. Classic approaches include distance-based methods [Breunig *et al.*, 2000; Yeh *et al.*, 2016; Liu *et al.*, 2008] that identify outliers based on their proximity to normal data groups, density estimation [Goldstein and Dengel, 2012; Zong *et al.*, 2018] that spots samples in low-density regions, and clustering-based methods [Yairi *et al.*, 2001; He *et al.*, 2003; Qiu *et al.*, 2025b] that group normal patterns and identify deviations. Tests from the TAB benchmark [Qiu *et al.*, 2025a] show these traditional methods often beat deep learning at finding pattern anomalies, likely because they directly measure geometry and are sensitive to local structures.

Reconstruction-based Methods

Reconstruction methods work on a simple idea: models trained on normal data make larger errors when they see abnormal patterns [Sakurada and Yairi, 2014; Kingma and Welling, 2013]. These methods have evolved with deep learning, starting with basic autoencoders [Niu *et al.*, 2020; Sakurada and Yairi, 2014], then recurrent networks [Niu *et al.*, 2020; Su *et al.*, 2019; Bhatnagar *et al.*, 2021], and now attention-based models [Xu *et al.*, 2021; Shentu *et al.*, 2025]. Deep learning methods, especially Transformers [Xu *et al.*, 2021; Yang *et al.*, 2023b; Wu *et al.*, 2022; Nie *et al.*, 2023; Liu *et al.*, 2024], have succeeded greatly due to their powerful representation advantages and are good at finding point anomalies. They learn complex features that catch single-point errors and local context problems [Qiu *et al.*, 2025a; Shentu *et al.*, 2025]. However, these complex models can fail with simple outliers [Zeng *et al.*, 2023] and struggle with pattern anomalies because they focus too much on local quality and miss long-term shifts.

Discriminative Learning Methods

Discriminative methods learn boundaries between normal and abnormal regions directly. One-class classification [Schölkopf *et al.*, 1999] builds tight boundaries around normal data in feature spaces. Contrastive learning [Yang *et al.*, 2023b; Yue *et al.*, 2022; Zhuang *et al.*, 2025; Ruff *et al.*, 2019] creates useful features by checking consistency across different views without needing anomaly labels. But these methods have problems: without real anomalies for training, they must create fake ones that might not match real patterns. The learned boundaries might only work for specific anomaly types seen during training, making new anomaly patterns hard to handle.

2.2 Joint Temporal-Frequency Domain Analysis

Frequency analysis finds anomalies that time-based methods miss, including broken cycles, warped harmonics, and spectral problems [Ren *et al.*, 2019; Thill *et al.*, 2017]. Different anomalies show up better in different domains: seasonal anomalies appear clearly in the frequency domain as broken patterns, while trend anomalies show better in the temporal domain as long-term shifts [Qiu *et al.*, 2025a].

Early work focused on single-variable spectral analysis [Feng *et al.*, 2021; Ren *et al.*, 2019] using frequency maps and partial Fourier transforms to find anomalies. Modern methods [Wu *et al.*, 2022; Yang *et al.*, 2023b; Nam *et al.*, 2024; Wu *et al.*, 2024; Wang *et al.*, 2025] try to combine temporal and frequency analysis but face several challenges: temporal and frequency details do not always match, high-frequency information gets lost during processing, and cross-channel relationships are hard to model [Wu *et al.*, 2024]. Current fusion methods just combine features or merge them late, failing to model the complex links between temporal and frequency scores.

3 Methodology

3.1 Problem Formulation

Consider a time series $\mathcal{X} = \langle x_1, x_2, \ldots, x_T \rangle$, where each point $x_t \in \mathbb{R}^d$ represents a d-dimensional measurement at time t. The training data $\mathcal{X}$ is assumed to contain only normal behavior patterns [Chandola *et al.*, 2009; Lai *et al.*,

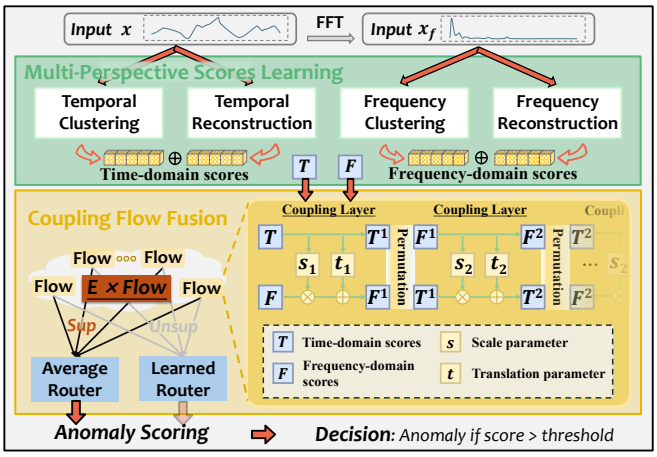

Figure 1: Architecture of FlowFuse. The framework processes time series through FFT transformation for dual-domain analysis, parallel multi-view scoring, coupling flow-based probabilistic fusion with alternating coupling layers, and flexible routing strategies for anomaly scoring.

2021]. Our goal is to build a detector that identifies anomalies in test sequences $\mathcal{X}_{\text{test}}$, producing binary labels $\mathcal{Y}_{\text{test}} = \langle y_1, y_2, \ldots, y_{T'} \rangle$ where $y_t \in \{0, 1\}$ indicates normal (0) or abnormal (1) behavior.

3.2 Framework Overview

FlowFuse is a multi-view time series anomaly detection framework comprising three core stages:

1. **Multi-Perspective Scores Learning:** The input time series is processed simultaneously in temporal and frequency domains through FFT transformation. Four parallel detectors (Temporal Clustering, Temporal Reconstruction, Frequency Clustering, and Frequency Reconstruction) extract complementary anomaly scores, yielding temporal scores $\mathbf{T}$ and frequency scores $\mathbf{F}$.
2. **Coupling Flow Fusion:** An ensemble of E coupling flows models the joint distribution of multi-view scores. Each coupling flow learns complex dependencies between temporal and frequency scores through alternating coupling layers with scale and translation transformations.
3. **Anomaly Scoring:** In unsupervised settings, an average router performs ensemble averaging across all flows. When labeled data is available, a learned router adaptively weights ensemble members based on score uncertainty. The final anomaly decision is made by comparing scores against a threshold.

Figure 1 illustrates the overall architecture. The framework first extracts anomaly scores from four complementary perspectives—clustering and reconstruction methods in both temporal and frequency domains—to capture diverse anomaly characteristics. These multi-view scores are then processed by an ensemble of coupling flows that learn their joint distribution through invertible transformations, producing fused anomaly scores.

The key advantage of using multiple flows is that their score disagreement (variance) naturally quantifies detection uncertainty. High disagreement indicates samples near decision boundaries where the model has low confidence. This uncertainty measure serves dual purposes: it identifies the most informative samples for selective supervision, and it provides practitioners with confidence estimates for detection results. The design ensures the framework operates effectively in purely unsupervised settings while seamlessly incorporating supervision when available to enhance detection performance.

3.3 Multi-Perspective Scores Learning

The framework begins with standardization to ensure comparability across dimensions, followed by adaptive windowing that segments data using a **sliding window** approach with window length W and stride s, producing overlapping windows $\mathbf{W}_i \in \mathbb{R}^{W \times d}$. The window size W can be automatically determined through FFT-based periodicity detection to align with natural data cycles, or set manually based on domain knowledge. Each window is also transformed via FFT to obtain its frequency representation for parallel processing in both temporal and frequency domains. By default, we set $W = 50$ and $s = 1$ across all experiments.

The choice of four detection perspectives is guided by two orthogonal design dimensions:

Domain Dimension (Temporal vs. Frequency). Different anomaly types manifest distinctively across domains. Point anomalies and local contextual anomalies are more apparent in the temporal domain, while seasonal anomalies and harmonic distortions are more naturally captured in the frequency domain.

Paradigm Dimension (Clustering vs. Reconstruction). Clustering-based methods excel at detecting global outliers and novel patterns far from learned clusters. Reconstruction-based methods excel at detecting subtle local deviations through high reconstruction errors.

For each window, we compute anomaly scores from four complementary perspectives:

- **Temporal Clustering:** We apply K-means clustering to identify $C = 24$ typical temporal patterns (see Section 4.4) in the training data [Yairi *et al.*, 2001; He *et al.*, 2003]. For each test window, we compute its Euclidean distance to the nearest cluster center. Windows that fall far from all learned clusters likely represent anomalous patterns not seen during training.
- **Temporal Reconstruction:** We employ a Transformer model with inverted tokenization [Liu *et al.*, 2024; Nie *et al.*, 2023], where each variable's time series serves as a token rather than each time point. The model learns to reconstruct normal temporal patterns through self-attention mechanisms [Xu *et al.*, 2021]. High reconstruction errors indicate deviations from learned normal dependencies.
- **Frequency Clustering:** After applying FFT to convert windows to the frequency domain, we perform K-means clustering on the magnitude spectra with the same number of clusters C. This captures typical frequency patterns and identifies anomalies with unusual spectral characteristics that temporal analysis might miss [Ren *et al.*, 2019].
- **Frequency Reconstruction:** A specialized Transformer operates directly on frequency representations (both mag-

nitude and phase), learning to reconstruct normal spectral patterns. This method excels at detecting subtle frequency anomalies like broken periodicities, harmonic distortions, or abnormal frequency components [Thill *et al.*, 2017; Nam *et al.*, 2024; Wu *et al.*, 2024].

Using the same number of clusters C across both temporal and frequency domains ensures balanced representational capacity and consistent granularity, enabling fair integration of clustering-based scores from different perspectives. This multi-view approach leverages the observation that different anomaly types manifest distinctively across domains and detection paradigms. Point anomalies typically show high reconstruction errors, while pattern anomalies are better captured by clustering distances [Liu *et al.*, 2008].

Since we use overlapping sliding windows with stride s, each timestamp may appear in multiple windows. We aggregate these window-level scores to point-level through averaging:

$$s_t^{(v)} = \frac{1}{|\mathcal{W}_t|} \sum_{w \in \mathcal{W}_t} s_w^{(v)}, \tag{1}$$

where $\mathcal{W}_t$ denotes all windows containing timestamp t [Yeh *et al.*, 2016; Tatbul *et al.*, 2018], and $v \in \{1, 2, 3, 4\}$ indexes the four views. The resulting score matrix $\mathbf{S}_t \in \mathbb{R}^{d \times 4}$ for each timestamp provides a comprehensive characterization of potential anomalies from multiple perspectives, where each row corresponds to one dimension and each column represents one of the four detection views.

Given the score matrix $\mathbf{S}_t \in \mathbb{R}^{d \times 4}$, we partition it along the column dimension into:

- Temporal scores: $\mathbf{T}_t = \mathbf{S}_t[:, 1{:}2] \in \mathbb{R}^{d \times 2}$ (clustering + reconstruction)
- Frequency scores: $\mathbf{F}_t = \mathbf{S}_t[:, 3{:}4] \in \mathbb{R}^{d \times 2}$ (clustering + reconstruction)

3.4 Coupling Flow Fusion

Traditional score aggregation methods fail to capture the complex dependencies between different detection methods. Table 1 summarizes the limitations of common approaches.

Method	Non-linear Modeling	Cross-view Interaction	Distribution Learning
Average	✗	✗	✗
Maximum	✗	✗	✗
Learned Weights	✗	✗	✗
MLP Fusion	✓	✓	✗
Coupling Flow (Ours)	✓	✓	✓

Table 1: Comparison of score fusion strategies.

Linear methods (averaging, maximum, learned weights) treat views independently, ignoring their correlations. While MLP-based fusion can model non-linear interactions, it lacks principled density estimation and cannot determine whether a score pattern is normal or anomalous based on the learned distribution. Consider two scenarios: (1) A sample with high temporal but low frequency scores might indicate a temporal anomaly that frequency methods correctly ignore, and averaging dilutes this signal. (2) Moderate scores across all views might indicate a true anomaly through consistent deviation; maximum selection misses this pattern.

Coupling flows address these limitations by modeling the *joint distribution* $p(\mathbf{S})$ of multi-view scores through invertible transformations with tractable likelihood computation. Samples with low likelihood under the learned normal distribution are identified as anomalies. Since the entire process operates without anomaly labels, this approach performs unsupervised modeling of the complete joint distribution.

Before fusion, all scores are standardized within each variable to zero mean and unit variance, ensuring comparability across different detection methods. Each coupling flow $f_e : \mathbb{R}^{d \times 4} \to \mathbb{R}^{d \times 4}$ consists of L_c coupling layers that progressively transform the complex score distribution to a standard Gaussian distribution in latent space.

Coupling Layer Architecture. Each coupling layer applies conditional affine transformations through an alternating scheme. Given the temporal and frequency partitions $[\mathbf{T}_t^{(\ell)}, \mathbf{F}_t^{(\ell)}]$ at layer ℓ, a single coupling block performs:

Step 1: Update frequency scores conditioned on temporal scores:

$$\begin{aligned} \mathbf{T}_t^{(\ell+\frac{1}{2})} &= \mathbf{T}_t^{(\ell)}, \\ \mathbf{F}_t^{(\ell+\frac{1}{2})} &= \mathbf{F}_t^{(\ell)} \odot \exp\big(\mathbf{s}_\theta(\mathbf{T}_t^{(\ell)})\big) + \mathbf{t}_\theta(\mathbf{T}_t^{(\ell)}), \end{aligned} \tag{2}$$

where $\mathbf{s}_\theta, \mathbf{t}_\theta : \mathbb{R}^{d \times 2} \to \mathbb{R}^{d \times 2}$ are scale and translation networks parameterized by θ, and $\odot$ denotes element-wise multiplication.

Step 2: Update temporal scores conditioned on updated frequency scores:

$$\begin{aligned} \mathbf{F}_t^{(\ell+1)} &= \mathbf{F}_t^{(\ell+\frac{1}{2})}, \\ \mathbf{T}_t^{(\ell+1)} &= \mathbf{T}_t^{(\ell+\frac{1}{2})} \odot \exp\big(\mathbf{s}_\phi(\mathbf{F}_t^{(\ell+\frac{1}{2})})\big) + \mathbf{t}_\phi(\mathbf{F}_t^{(\ell+\frac{1}{2})}), \end{aligned} \tag{3}$$

where $\mathbf{s}_\phi, \mathbf{t}_\phi : \mathbb{R}^{d \times 2} \to \mathbb{R}^{d \times 2}$ are parameterized by ϕ.

This alternating structure enables bidirectional modeling of dependencies between temporal and frequency domains. The key insight is that by using the *updated* values from the previous half-step (e.g., $\mathbf{F}_t^{(\ell+\frac{1}{2})}$ instead of $\mathbf{F}_t^{(\ell)}$), the flow can learn complex interactions—how temporal scores relate to frequency scores that have already been contextualized by temporal information.

The complete coupling flow consists of L_c such blocks stacked sequentially:

$$\mathbf{z}_t = f_e(\mathbf{S}_t) = f_e^{(L_c)} \circ \cdots \circ f_e^{(2)} \circ f_e^{(1)}(\mathbf{S}_t), \tag{4}$$

where $\mathbf{z}_t \in \mathbb{R}^{d \times 4}$ is the latent representation. Each layer progressively refines the representation, with later layers capturing higher-order dependencies between views.

Ensemble Strategy. We train an ensemble of E coupling flows $\{f_1, \ldots, f_E\}$ with different random initializations and data subsets to create diversity. Each flow independently optimizes the negative log-likelihood of observed score patterns:

$$\mathcal{L}_{\text{flow}}^{(e)} = \frac{1}{N} \sum_{t=1}^{N} \left[\frac{1}{2} \|\mathbf{z}_t^{(e)}\|_F^2 - \log \left| \det J_{f_e}(\mathbf{S}_t) \right| \right], \tag{5}$$

where $\mathbf{z}_t^{(e)} = f_e(\mathbf{S}_t)$ is the latent representation, $\|\cdot\|_F$ denotes the Frobenius norm, and J_{f_e} is the Jacobian matrix of the flow transformation. The first term encourages latent representations to follow a standard Gaussian distribution, while the Jacobian determinant ensures invertibility.

The ensemble improves robustness through model averaging, provides more accurate density estimation with lower variance, and naturally quantifies detection uncertainty through score disagreement $u_t = \mathrm{Var}_{e=1}^{E}[r_e(\mathbf{S}_t)]$. High variance indicates samples near decision boundaries where individual flows disagree. We adopt $E = 4$ and $L_c = 2$ as default across all experiments.

To obtain interpretable anomaly scores, we convert likelihoods to percentile ranks. During training, we store the likelihood distribution for each flow. At test time, for sample $\mathbf{S}_t$:

$$r_e(\mathbf{S}_t) = \frac{1}{N}\sum_{i=1}^{N} \mathbb{I}\left[\mathcal{L}_{\text{flow}}^{(e)}(\mathbf{S}_t) > \mathcal{L}_{\text{flow}}^{(e)}(\mathbf{S}_i^{\text{train}})\right], \quad (6)$$

where $\mathbb{I}[\cdot]$ is the indicator function and $r_e(\mathbf{S}_t) \in [0, 1]$.

3.5 Anomaly Scoring

The final anomaly score adapts to the availability of supervision through two routing strategies. In the unsupervised setting, we use an average router that performs ensemble averaging:

$$\bar{r}(\mathbf{S}_t) = \frac{1}{E}\sum_{e=1}^{E} r_e(\mathbf{S}_t). \quad (7)$$

When labeled data becomes available, FlowFuse can optionally employ a learned router that leverages the ensemble's uncertainty measure. We select the top-K highest-uncertainty samples where $K = \lceil p_{\text{train}} \cdot N_{\text{train}} \rceil$, and train a lightweight routing network $g_\psi : \mathbb{R}^{d\times 4} \to \mathbb{R}^E$ that assigns weights to ensemble members:

$$w_e(\mathbf{S}_t) = \frac{\exp(g_\psi(\mathbf{S}_t)_e/\tau)}{\sum_{e'=1}^{E}\exp(g_\psi(\mathbf{S}_t)_{e'}/\tau)}. \quad (8)$$

The router is trained using ranking loss on anomaly-normal pairs from the high-uncertainty subset:

$$\mathcal{L}_{\text{rank}} = \frac{1}{|\mathcal{P}|}\sum_{(i,j)\in\mathcal{P}} \log\left(1 + \exp\left(\phi(\mathbf{S}_j) - \phi(\mathbf{S}_i)\right)\right), \quad (9)$$

where $\phi(\mathbf{S}_t) = \sum_{e=1}^{E} w_e(\mathbf{S}_t) \cdot r_e(\mathbf{S}_t)$ is the router-weighted score. This focuses limited labels on ambiguous regions where supervision has maximum impact.

The ensemble average $\bar{r}(\mathbf{S}_t)$ provides robust anomaly scores by aggregating anomaly scores from diverse coupling flows. The weighted score $\phi(\mathbf{S}_t)$ adaptively combines ensemble members based on the input score pattern, improving detection in previously ambiguous regions. This design ensures FlowFuse operates effectively across the full spectrum from purely unsupervised to semi-supervised settings.

4 Experiment

4.1 Experimental Settings

Datasets

We evaluate FlowFuse on 18 diverse benchmarks covering 10 univariate and 8 multivariate datasets across multiple domains including spacecraft telemetry, server monitoring, healthcare, movement analysis, and industrial systems. These datasets exhibit varied characteristics in dimensionality (1–55 channels), sequence lengths (785–1,416,825 points), and anomaly ratios (0.20%–15.57%), ensuring robust validation across different operational contexts. Table 2 summarizes all dataset statistics with original sources.

Dataset	Domain	Dim	Series	Avg Total Length	Avg Test Length	Avg AR (%)	Train AR (%)
GAIA	AIOps	1	184	9,777	8,799	1.26	0.19
GHL	Machinery	1	1	200,001	180,001	0.43	0.00
KDD21	Multiple	1	243	65,903	47,294	0.58	0.00
MGAB	Synthetic	1	6	100,000	90,000	0.20	0.00
NASA-MSL	Spacecraft	1	22	5,167	2,897	3.85	0.00
NAB	Multiple	1	45	7,115	3,557	9.84	6.55
OPPORTUNITY	Movement	1	462	31,359	28,223	4.12	19.11
NASA-SMAP	Spacecraft	1	35	10,539	7,930	2.20	0.00
SVDB	Health	1	52	230,400	207,360	4.87	5.48
YAHOO	Multiple	1	346	1,570	785	0.63	0.46
LTDB	Health	2	5	100,000	87,285	15.57	11.72
MITDB	Health	2	6	141,667	106,250	2.72	0.00
MSL	Spacecraft	55	1	132,046	73,729	5.88	0.00
SMD	Server	38	1	1,416,825	708,420	2.08	0.00
NYC	Transport	3	1	17,520	4,416	0.57	0.00
PSM	Server	25	1	220,322	87,841	11.07	0.00
SMAP	Spacecraft	25	1	562,800	427,617	9.72	0.00
SVDB	Health	2	6	110,133	86,373	3.14	5.48

Dataset types distinguished by row color: Cyan = 10 Univariate (GAIA–YAHOO); Yellow = 8 Multivariate (LTDB–SVDB).

Table 2: Summary of evaluation datasets. AR denotes anomaly ratio.

Baselines

We compare against 18 state-of-the-art methods spanning three major anomaly detection paradigms: statistical distribution-based approaches (6 methods), reconstruction-based methods (10 methods), and discriminative learning approaches (2 methods), as detailed in Table 4. The baselines encompass non-learning statistical methods, traditional machine learning algorithms, and modern deep learning architectures.

Setup

We utilize TAB [Qiu *et al.*, 2025a] for unified evaluation, with all baseline results derived from the same framework. To ensure fair comparison and demonstrate robustness, we employ a single set of hyperparameters for all univariate datasets and another for all multivariate datasets, without dataset-specific tuning. We adopt two evaluation metrics: *Affiliated F1-score* [Huet *et al.*, 2022] for label-based evaluation and AUROC for score-based evaluation. Hyperparameter configurations are detailed in Section 4.4.

4.2 Main Results

Table 3 presents evaluation results on both univariate and multivariate datasets, distinguished by background color (cyan for univariate, yellow for multivariate). FlowFuse achieves the best performance on the majority of benchmarks, demonstrating strong generalization across diverse anomaly detection scenarios.

For univariate time series, FlowFuse obtains impressive results on challenging datasets with complex temporal patterns (e.g., GHL, SMAP, YAHOO), while maintaining consistent superiority in ranking quality as measured by AUC-ROC. On multivariate benchmarks, our method delivers robust performance by effectively capturing cross-dimensional dependen-

Dataset	Metric	Ours	Modern	DualTF	iTrans	ATrans	DC	TranAD	ConAD	Patch	DLin	VAE	DAGMM	KNN	KMeans	OCSVM	IF	DP	LOF	HBOS
GAIA	Aff-F	0.871	0.904	0.753	**0.907**	0.697	0.711	0.790	0.683	0.902	0.897	0.727	0.598	0.759	0.781	0.725	0.731	0.673	0.737	0.689
	A-R	**0.872**	0.821	0.564	0.823	0.446	0.411	0.756	0.486	0.819	0.801	0.748	0.648	0.821	0.738	0.726	0.695	0.755	0.817	0.687
GHL	Aff-F	**0.975**	0.723	0.682	0.709	0.652	0.669	0.577	0.667	0.735	0.730	0.555	0.465	0.679	0.598	0.667	0.687	0.667	0.679	0.638
	A-R	**0.998**	0.493	0.374	0.498	0.476	0.498	0.020	0.500	0.500	0.528	0.087	0.020	0.751	0.747	0.751	0.500	0.888	0.751	0.662
KDD21	Aff-F	**0.895**	0.718	0.698	0.767	0.698	0.686	0.723	0.685	0.713	0.726	0.652	0.640	0.678	0.822	0.669	0.675	0.667	0.675	0.666
	A-R	**0.887**	0.534	0.569	0.605	0.499	0.493	0.528	0.502	0.529	0.538	0.540	0.538	0.638	0.778	0.590	0.554	0.532	0.584	0.564
MGAB	Aff-F	**0.793**	0.678	0.675	0.691	0.671	0.673	0.670	0.667	0.669	0.668	0.664	0.620	0.666	0.688	0.666	0.664	0.667	0.667	0.665
	A-R	**0.773**	0.561	0.576	0.501	0.500	0.504	0.592	0.522	0.559	0.567	0.555	0.545	0.560	0.605	0.550	0.487	0.515	0.509	0.586
MSL	Aff-F	**0.922**	0.896	0.766	0.865	0.743	0.757	0.902	0.673	0.883	0.903	0.686	0.609	0.775	0.894	0.795	0.658	0.673	0.772	0.733
	A-R	**0.803**	0.726	0.537	0.724	0.426	0.469	0.616	0.500	0.727	0.710	0.652	0.609	0.673	0.725	0.666	0.561	0.636	0.614	0.607
NAB	Aff-F	0.828	0.838	0.782	0.832	0.751	0.714	**0.858**	0.701	0.848	0.850	0.739	0.620	0.730	0.818	0.722	0.711	0.680	0.695	0.744
	A-R	**0.640**	0.612	0.550	0.614	0.469	0.506	0.546	0.506	0.605	0.608	0.556	0.572	0.563	0.626	0.584	0.535	0.531	0.545	0.570
OPP	Aff-F	**0.788**	0.733	0.710	0.709	0.728	0.679	0.762	0.770	0.732	0.737	0.674	0.628	0.656	0.734	0.654	0.654	0.667	0.671	0.653
	A-R	0.664	0.215	0.411	0.224	**0.665**	0.503	0.559	0.504	0.217	0.304	0.514	0.578	0.461	0.285	0.487	0.242	0.260	0.545	0.522
SMAP	Aff-F	**0.967**	0.913	0.686	0.928	0.764	0.760	0.851	0.680	0.906	0.906	0.595	0.569	0.717	0.886	0.698	0.655	0.674	0.711	0.647
	A-R	**0.899**	0.694	0.535	0.752	0.480	0.487	0.520	0.502	0.707	0.615	0.596	0.586	0.594	0.802	0.586	0.513	0.655	0.551	0.526
SVDB	Aff-F	**0.833**	0.733	0.745	0.718	0.686	0.685	0.730	0.682	0.727	0.728	0.683	0.611	0.710	0.735	0.698	0.672	0.682	0.709	0.700
	A-R	**0.780**	0.573	0.586	0.576	0.504	0.460	0.549	0.500	0.569	0.580	0.570	0.549	0.520	0.683	0.567	0.544	0.531	0.516	0.553
YAHOO	Aff-F	**0.914**	0.793	0.748	0.897	0.671	0.629	0.755	0.678	0.800	0.825	0.615	0.453	0.661	0.604	0.675	0.897	0.669	0.664	0.653
	A-R	**0.936**	0.804	0.467	0.891	0.477	0.490	0.697	0.488	0.828	0.843	0.756	0.707	0.734	0.589	0.639	0.924	0.862	0.754	0.678
LTDB	Aff-F	**0.794**	0.777	0.455	0.756	0.702	0.710	0.790	0.752	0.767	0.764	0.670	0.653	0.768	0.724	0.754	0.644	0.724	0.763	0.759
	A-R	**0.833**	0.619	0.589	0.579	0.505	0.494	0.590	0.576	0.587	0.599	0.610	0.545	0.632	0.738	0.615	0.559	0.551	0.621	0.611
MITDB	Aff-F	**0.925**	0.803	0.843	0.806	0.700	0.689	0.848	0.694	0.813	0.722	0.713	0.689	0.709	0.834	0.700	0.709	0.678	0.700	0.687
	A-R	**0.767**	0.663	0.693	0.679	0.424	0.503	0.691	0.488	0.676	0.583	0.667	0.682	0.692	0.692	0.689	0.618	0.598	0.627	0.681
MSL	Aff-F	**0.738**	0.726	0.258	0.705	0.685	0.674	0.724	0.671	0.714	0.723	0.642	0.723	0.696	0.580	0.641	0.584	0.677	0.701	0.680
	A-R	**0.645**	0.621	0.499	0.589	0.502	0.500	0.478	0.548	0.621	0.601	0.530	0.569	0.623	0.603	0.524	0.524	0.488	0.557	0.574
SMD	Aff-F	0.794	**0.839**	0.679	0.817	0.674	0.674	0.789	0.023	0.830	0.834	0.450	0.023	0.696	0.686	0.742	0.626	0.674	0.682	0.629
	A-R	**0.749**	0.721	0.703	0.745	0.509	0.500	0.663	0.491	0.736	0.708	0.641	0.527	0.716	0.713	0.602	0.664	0.672	0.645	0.626
NYC	Aff-F	**0.946**	0.693	0.676	0.683	0.732	0.674	0.796	0.714	0.805	0.725	0.767	0.694	0.644	0.646	0.667	0.648	0.668	0.652	0.675
	A-R	0.808	0.696	0.723	0.594	**0.859**	0.526	0.676	0.443	0.667	0.699	0.661	0.573	0.466	0.833	0.456	0.475	0.476	0.464	0.446
PSM	Aff-F	0.739	0.823	0.725	**0.855**	0.634	0.671	0.748	0.648	0.836	0.832	0.295	0.463	0.695	0.735	0.531	0.620	0.694	0.694	0.658
	A-R	0.635	0.587	0.544	0.583	0.499	0.499	0.635	0.533	0.583	0.559	0.642	0.637	**0.744**	0.732	0.619	0.542	0.539	0.730	0.714
SMAP	Aff-F	0.551	0.616	0.674	0.577	**0.692**	0.681	0.538	0.430	0.629	0.607	0.487	0.430	0.630	0.517	0.503	0.512	0.681	0.642	0.509
	A-R	0.468	0.434	0.465	0.409	0.501	0.500	0.369	0.364	0.441	0.391	0.412	0.573	**0.629**	0.405	0.393	0.487	0.429	0.626	0.585
SVDB	Aff-F	**0.896**	0.746	0.585	0.746	0.701	0.711	0.752	0.694	0.787	0.727	0.697	0.692	0.733	0.820	0.723	0.708	0.692	0.734	0.735
	A-R	**0.913**	0.593	0.555	0.636	0.491	0.464	0.577	0.533	0.651	0.610	0.570	0.564	0.595	0.839	0.585	0.533	0.527	0.580	0.568

Dataset types distinguished by row color: Cyan = 10 Univariate (GAIA–YAHOO); Yellow = 8 Multivariate (LTDB–SVDB).

Table 3: Average AUC-ROC (A-R) and Affiliated-F1 (Aff-F) accuracy measures for all datasets. Best results in **Red**, second-best Blue.

Paradigm	Method	Abbrev.
Statistical Distribution-based	• LOF [Breunig *et al.*, 2000]	LOF
	• KNN	KNN
	• Isolation Forest [Liu *et al.*, 2008]	IF
	• HBOS [Goldstein and Dengel, 2012]	HBOS
	• OC-SVM [Schölkopf *et al.*, 1999]	OCSVM
	• K-Means [Yairi *et al.*, 2001]	KMeans
Reconstruction-based	• VAE [Kingma and Welling, 2013]	VAE
	• DAGMM [Zong *et al.*, 2018]	DAGMM
	• DeepPoint [Bhatnagar *et al.*, 2021]	DP
	• TranAD [Tuli *et al.*, 2022]	TranAD
	• Anomaly Transformer [Xu *et al.*, 2021]	ATrans
	• DualTF [Nam *et al.*, 2024]	DualTF
	• PatchTST [Nie *et al.*, 2023]	Patch
	• ModernTCN [Luo and Wang, 2024]	Modern
	• DLinear [Zeng *et al.*, 2023]	DLin
	• iTransformer [Liu *et al.*, 2024]	iTrans
Discriminative Learning	• DCdetector [Yang *et al.*, 2023b]	DC
	• ContraAD [Zhuang *et al.*, 2025]	ConAD

• Non-Learning • Machine Learning • Deep Learning

Table 4: Baseline methods organized by detection paradigm.

Variations		LTDB	MSL	SMAP	SVDB	Avg.
Simple Averaging		0.745	0.683	0.433	0.798	0.665
Multi-View Scores	w/o Temporal Clustering	0.721	0.652	0.412	0.785	0.643
	w/o Temporal Reconstruction	0.726	0.715	0.368	0.800	0.652
	w/o Frequency Clustering	0.755	0.698	0.527	0.801	0.695
	w/o Frequency Reconstruction	0.768	0.710	0.522	0.785	0.696
FlowFuse (Full)		**0.794**	**0.738**	**0.551**	**0.896**	**0.745**

Table 5: Ablation studies for FlowFuse in terms of Aff-F1.

cies through the coupling flow mechanism, achieving top results on LTDB, MITDB, NYC, and SVDB.

Compared to recent deep learning methods such as ModernTCN, DualTF, and Anomaly Transformer, FlowFuse demonstrates more stable performance across different data characteristics. While these baseline methods often excel on specific datasets but struggle on others, our approach maintains competitive results throughout all 18 benchmarks, validating the effectiveness of multi-view ensemble fusion.

4.3 Ablation Studies

To validate the contribution of each component in FlowFuse, we conduct comprehensive ablation studies on four representative datasets. Table 5 presents the results.

The results demonstrate that: (1) coupling flow fusion significantly outperforms simple averaging (+8.0% on average), validating the importance of modeling non-linear score dependencies; (2) each multi-view component contributes to overall performance, with temporal views showing larger impact than frequency views on most datasets; (3) the full model achieves the best results, confirming the complementary nature of all four detection perspectives.

4.4 Further Analysis

Method-Specific Detection Bias

To illustrate multi-view fusion rationale, we analyze 35 methods spanning three detection paradigms (listed in our repository) on datasets grouped by anomaly types. Figure 2 presents

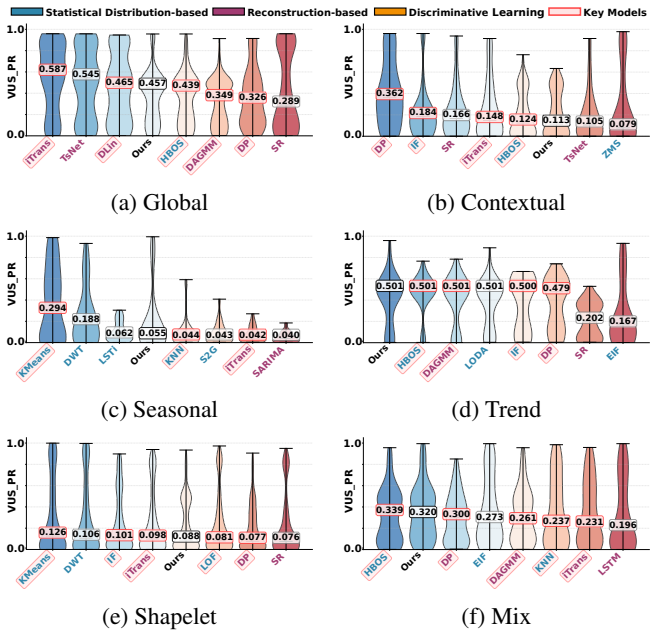

Figure 2: Performance distributions of 35 methods across six anomaly types. Top performers vary significantly across categories, revealing method-specific detection biases.

VUS-PR performance distributions across six anomaly categories, each subfigure visualizing method performance variation for a specific type.

Notably, we observe distinct paradigm tendencies: deep learning methods (e.g., iTransformer [Liu *et al.*, 2024], DLinear [Zeng *et al.*, 2023]) work effectively for point anomalies (global, contextual; Figure 2(a)(b)), while statistical approaches (e.g., KMeans, DWT [Thill *et al.*, 2017], HBOS) are more suitable for subsequence anomalies (seasonal, shapelet; Figure 2(c)(e)). Additionally, even top-performing methods achieve only moderate performance on mixed anomalies (Figure 2(f)), lower than their performance on single-type anomalies.

This observation supports FlowFuse's multi-view fusion design. Integrating complementary perspectives via coupling flows, FlowFuse maintains stable performance across all six categories, alleviating constraints of type-specialized detection methods. The complete list of 35 methods and their implementations is available in our repository.

Optional Supervised Enhancement

When labeled data is available, FlowFuse can optionally refine detection through uncertainty-guided supervision. Table 6 shows performance with varying label ratios.

The results reveal that: (1) unsupervised FlowFuse already achieves strong baseline performance; (2) small amounts of labeled data (1–5%) yield substantial improvements, with diminishing returns at higher ratios; (3) performance saturates quickly, validating the uncertainty-guided sample selection strategy that focuses supervision on the most informative samples.

Dataset	Unsup. (0%)	Label Ratio (%) 1	5	20	50	100
NAB	0.640	0.680	0.700	0.710	0.700	0.703
SVDB	0.780	0.810	0.820	0.820	0.820	0.820
YAHOO	0.936	0.941	0.945	0.944	0.945	0.945
LTDB	0.833	0.847	0.853	0.858	0.860	0.857

Table 6: Performance (AUC-ROC) with optional supervised enhancement. Baseline (0%) represents unsupervised FlowFuse.

Parameter Sensitivity

We investigate the sensitivity of FlowFuse to two key hyperparameters: the number of clusters C and the number of coupling flows E. Figure 3 presents the results on four benchmark datasets.

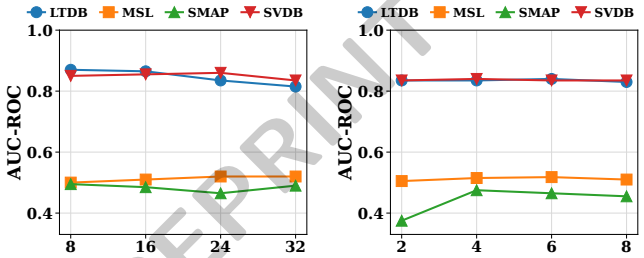

(a) C (clusters) (b) E (flows)

Figure 3: Parameter sensitivity analysis in terms of AUC-ROC.

For the number of clusters C, FlowFuse maintains stable performance across the range of 8 to 32, with less than 3% variation for most datasets. For the number of flows E, performance improves from $E = 2$ to $E = 4$ then saturates, indicating diminishing returns from additional ensemble members. We adopt $E = 4$ as the default. Overall, FlowFuse exhibits robust performance across its hyperparameter space without requiring precise tuning.

5 Conclusion

In this paper, we proposed FlowFuse, a multi-view ensemble framework that addresses anomaly diversity through coupling flow-based score fusion. By modeling the joint distribution of four complementary detection perspectives spanning temporal and frequency domains, as well as clustering and reconstruction paradigms, FlowFuse captures complex inter-view dependencies that linear aggregation cannot express. An ensemble of coupling flows provides robustness and natural uncertainty quantification, which enables targeted supervision when labels are available. Experiments on 18 benchmarks demonstrate state-of-the-art performance across diverse anomaly types, validating that principled multi-view fusion enables more comprehensive anomaly detection.

Ethical Statement

Our work uses only publicly available benchmark datasets without personally identifiable information. The proposed anomaly detection framework is for beneficial system reliability and safety monitoring applications, and no human subjects were involved in this research.

Acknowledgments

This work was partially supported by the National Natural Science Foundation of China (62372179) and the InnoHK funding.

Contribution Statement

Wanghui Qiu and Chenxi Liu contributed equally to this work as co-first authors. Bin Yang is the corresponding author.

References

[Bhatnagar *et al.*, 2021] Aadyot Bhatnagar, Paul Kassianik, Chenghao Liu, Tian Lan, Wenzhuo Yang, Rowan Cassius, Doyen Sahoo, Devansh Arpit, Sri Subramanian, Gerald Woo, Amrita Saha, Arun Kumar Jagota, Gokulakrishnan Gopalakrishnan, Manpreet Singh, K C Krithika, Sukumar Maddineni, Daeki Cho, Bo Zong, Yingbo Zhou, Caiming Xiong, Silvio Savarese, Steven Hoi, and Huan Wang. Merlion: A machine learning library for time series. 2021.

[Breunig *et al.*, 2000] Markus M Breunig, Hans-Peter Kriegel, Raymond T Ng, and Jörg Sander. Lof: identifying density-based local outliers. In *Proceedings of the 2000 ACM SIGMOD international conference on Management of data*, pages 93–104, 2000.

[Campos *et al.*, 2022] David Campos, Tung Kieu, Chenjuan Guo, Feiteng Huang, Kai Zheng, Bin Yang, and Christian S. Jensen. Unsupervised time series outlier detection with diversity-driven convolutional ensembles. *Proc. VLDB Endow.*, 15(3):611–623, 2022.

[Chandola *et al.*, 2009] Varun Chandola, Arindam Banerjee, and Vipin Kumar. Anomaly detection: A survey. *ACM computing surveys*, 41(3):1–58, 2009.

[Feng *et al.*, 2021] Hsin-Yu Feng, Po-Ying Chen, and Janpu Hou. Sr-scatnet algorithm for on-device ecg time series anomaly detection. In *SoutheastCon 2021*, pages 1–5. IEEE, 2021.

[Goldstein and Dengel, 2012] Markus Goldstein and Andreas Dengel. Histogram-based outlier score (hbos): A fast unsupervised anomaly detection algorithm. *KI-2012: poster and demo track*, 1:59–63, 2012.

[Guo *et al.*, 2014] Chenjuan Guo, Christian S Jensen, and Bin Yang. Towards total traffic awareness. *ACM SIGMOD Record*, 43(3):18–23, 2014.

[He *et al.*, 2003] Zengyou He, Xiaofei Xu, and Shengchun Deng. Discovering cluster-based local outliers. *Pattern recognition letters*, 24(9-10):1641–1650, 2003.

[Huang *et al.*, 2022] Xuanwen Huang, Yang Yang, Yang Wang, Chunping Wang, Zhisheng Zhang, Jiarong Xu, Lei Chen, and Michalis Vazirgiannis. Dgraph: A large-scale financial dataset for graph anomaly detection. In *NeurIPS*, pages 22765–22777, 2022.

[Huet *et al.*, 2022] Alexis Huet, Jose Manuel Navarro, and Dario Rossi. Local evaluation of time series anomaly detection algorithms. In *SIGKDD*, pages 635–645, 2022.

[Hundman *et al.*, 2018] Kyle Hundman, Valentino Constantinou, Christopher Laporte, Ian Colwell, and Tom Soderstrom. Detecting spacecraft anomalies using lstms and nonparametric dynamic thresholding. In *SIGKDD*, pages 387–395, 2018.

[Kingma and Welling, 2013] Diederik P Kingma and Max Welling. Auto-encoding variational bayes. *arXiv preprint arXiv:1312.6114*, 2013.

[Lai *et al.*, 2021] Kwei-Herng Lai, Daochen Zha, Junjie Xu, Yue Zhao, Guanchu Wang, and Xia Hu. Revisiting time series outlier detection: Definitions and benchmarks. In *Proceedings of the conference on neural information processing systems datasets and benchmarks track (round 1)*, 2021.

[Liu *et al.*, 2008] Fei Tony Liu, Kai Ming Ting, and Zhi-Hua Zhou. Isolation forest. In *2008 eighth ieee international conference on data mining*, pages 413–422. IEEE, 2008.

[Liu *et al.*, 2024] Yong Liu, Tengge Hu, Haoran Zhang, Haixu Wu, Shiyu Wang, Lintao Ma, and Mingsheng Long. itransformer: Inverted transformers are effective for time series forecasting. In *ICLR*, 2024.

[Lu *et al.*, 2011] Hua Lu, Bin Yang, and Christian S Jensen. Spatio-temporal joins on symbolic indoor tracking data. In *2011 IEEE 27th International Conference on Data Engineering*, pages 816–827. IEEE, 2011.

[Luo and Wang, 2024] Donghao Luo and Xue Wang. Moderntcn: A modern pure convolution structure for general time series analysis. In *ICLR*, 2024.

[Ma *et al.*, 2014] Yu Ma, Bin Yang, and Christian S Jensen. Enabling time-dependent uncertain eco-weights for road networks. In *Proceedings of Workshop on Managing and Mining Enriched Geo-Spatial Data*, pages 1–6, 2014.

[Mathur and Tippenhauer, 2016] Aditya P Mathur and Nils Ole Tippenhauer. Swat: A water treatment testbed for research and training on ics security. In *CySWater*, pages 31–36, 2016.

[Nam *et al.*, 2024] Youngeun Nam, Susik Yoon, Yooju Shin, Minyoung Bae, Hwanjun Song, Jae-Gil Lee, and Byung Suk Lee. Breaking the time-frequency granularity discrepancy in time-series anomaly detection. In *WWW*, pages 4204–4215. ACM, 2024.

[Nie *et al.*, 2023] Yuqi Nie, Nam H. Nguyen, Phanwadee Sinthong, and Jayant Kalagnanam. A time series is worth 64 words: Long-term forecasting with transformers. In *ICLR*, 2023.

[Niu *et al.*, 2020] Zijian Niu, Ke Yu, and Xiaofei Wu. Lstm-based vae-gan for time-series anomaly detection. *Sensors*, 20(13):3738, 2020.

[Qiu *et al.*, 2025a] Xiangfei Qiu, Zhe Li, Wanghui Qiu, Shiyan Hu, Lekui Zhou, Xingjian Wu, Zhengyu Li, Chenjuan Guo, Aoying Zhou, Zhenli Sheng, et al. Tab: Unified benchmarking of time series anomaly detection methods. *arXiv preprint arXiv:2506.18046*, 2025.

[Qiu *et al.*, 2025b] Xiangfei Qiu, Xingjian Wu, Yan Lin, Chenjuan Guo, Jilin Hu, and Bin Yang. DUET: Dual clustering enhanced multivariate time series forecasting. In *SIGKDD*, pages 1185–1196, 2025.

[Ren *et al.*, 2019] Hansheng Ren, Bixiong Xu, Yujing Wang, Chao Yi, Congrui Huang, Xiaoyu Kou, Tony Xing, Mao Yang, Jie Tong, and Qi Zhang. Time-series anomaly detection service at microsoft. In *SIGKDD*, pages 3009–3017, 2019.

[Ruff *et al.*, 2019] Lukas Ruff, Robert A Vandermeulen, Nico Görnitz, Alexander Binder, Emmanuel Müller, Klaus-Robert Müller, and Marius Kloft. Deep semi-supervised anomaly detection. *arXiv preprint arXiv:1906.02694*, 2019.

[Sakurada and Yairi, 2014] Mayu Sakurada and Takehisa Yairi. Anomaly detection using autoencoders with nonlinear dimensionality reduction. In *MLSDA*, pages 4–11, 2014.

[Schölkopf *et al.*, 1999] Bernhard Schölkopf, Robert C Williamson, Alex Smola, John Shawe-Taylor, and John Platt. Support vector method for novelty detection. In *NeurIPS*, volume 12, 1999.

[Shentu *et al.*, 2025] Qichao Shentu, Beibu Li, Kai Zhao, Yang Shu, Zhongwen Rao, Lujia Pan, Bin Yang, and Chenjuan Guo. Towards a general time series anomaly detector with adaptive bottlenecks and dual adversarial decoders. In *ICLR*, 2025.

[Su *et al.*, 2019] Ya Su, Youjian Zhao, Chenhao Niu, Rong Liu, Wei Sun, and Dan Pei. Robust anomaly detection for multivariate time series through stochastic recurrent neural network. In *Proceedings of the 25th ACM SIGKDD international conference on knowledge discovery & data mining*, pages 2828–2837, 2019.

[Tatbul *et al.*, 2018] Nesime Tatbul, Tae Jun Lee, Stan Zdonik, Mejbah Alam, and Justin Gottschlich. Precision and recall for time series. *NeurIPS*, 31, 2018.

[Thill *et al.*, 2017] Markus Thill, Wolfgang Konen, and Thomas Bäck. Time series anomaly detection with discrete wavelet transforms and maximum likelihood estimation. In *ITISE*, volume 2, pages 11–23, 2017.

[Tuli *et al.*, 2022] Shreshth Tuli, Giuliano Casale, and Nicholas R Jennings. Tranad: Deep transformer networks for anomaly detection in multivariate time series data. *arXiv preprint arXiv:2201.07284*, 2022.

[von Birgelen and Niggemann, 2018] Alexander von Birgelen and Oliver Niggemann. Anomaly detection and localization for cyber-physical production systems with self-organizing maps. *IMPROVE-Innovative Modelling Approaches for Production Systems to Raise Validatable Efficiency: Intelligent Methods for the Factory of the Future*, pages 55–71, 2018.

[Wang *et al.*, 2025] Hao Wang, Licheng Pan, Zhichao Chen, Degui Yang, Sen Zhang, Yifei Yang, Xinggao Liu, Haoxuan Li, and Dacheng Tao. FreDF: Learning to forecast in the frequency domain. In *ICLR*, 2025.

[Wu *et al.*, 2022] Haixu Wu, Tengge Hu, Yong Liu, Hang Zhou, Jianmin Wang, and Mingsheng Long. Timesnet: Temporal 2d-variation modeling for general time series analysis. *arXiv preprint arXiv:2210.02186*, 2022.

[Wu *et al.*, 2024] Xingjian Wu, Xiangfei Qiu, Zhengyu Li, Yihang Wang, Jilin Hu, Chenjuan Guo, Hui Xiong, and Bin Yang. Catch: Channel-aware multivariate time series anomaly detection via frequency patching. *arXiv preprint arXiv:2410.12261*, 2024.

[Xu *et al.*, 2021] Jiehui Xu, Haixu Wu, Jianmin Wang, and Mingsheng Long. Anomaly transformer: Time series anomaly detection with association discrepancy. *arXiv preprint arXiv:2110.02642*, 2021.

[Yairi *et al.*, 2001] Takehisa Yairi, Yoshikiyo Kato, and Koichi Hori. Fault detection by mining association rules from house-keeping data. In *i-SAIRAS*, volume 3, 2001.

[Yang *et al.*, 2023a] Sean Bin Yang, Jilin Hu, Chenjuan Guo, Bin Yang, and Christian S Jensen. Lightpath: Lightweight and scalable path representation learning. In *SIGKDD*, pages 2999–3010, 2023.

[Yang *et al.*, 2023b] Yiyuan Yang, Chaoli Zhang, Tian Zhou, Qingsong Wen, and Liang Sun. Dcdetector: Dual attention contrastive representation learning for time series anomaly detection. In *Proceedings of the 29th ACM SIGKDD conference on knowledge discovery and data mining*, pages 3033–3045, 2023.

[Yeh *et al.*, 2016] Chin-Chia Michael Yeh, Yan Zhu, Liudmila Ulanova, Nurjahan Begum, Yifei Ding, Hoang Anh Dau, Diego Furtado Silva, Abdullah Mueen, and Eamonn Keogh. Matrix profile i: all pairs similarity joins for time series: a unifying view that includes motifs, discords and shapelets. In *2016 IEEE 16th international conference on data mining (ICDM)*, pages 1317–1322. Ieee, 2016.

[Yue *et al.*, 2022] Zhihan Yue, Yujing Wang, Juanyong Duan, Tianmeng Yang, Congrui Huang, Yunhai Tong, and Bixiong Xu. Ts2vec: Towards universal representation of time series. In *Proceedings of the AAAI conference on artificial intelligence*, volume 36, pages 8980–8987, 2022.

[Zamanzadeh Darban *et al.*, 2024] Zahra Zamanzadeh Darban, Geoffrey I Webb, Shirui Pan, Charu Aggarwal, and Mahsa Salehi. Deep learning for time series anomaly detection: A survey. *ACM Computing Surveys*, 57(1):1–42, 2024.

[Zeng *et al.*, 2023] Ailing Zeng, Muxi Chen, Lei Zhang, and Qiang Xu. Are transformers effective for time series forecasting? In *AAAI*, volume 37, pages 11121–11128, 2023.

[Zhuang *et al.*, 2025] Zhihao Zhuang, Yingying Zhang, Kai Zhao, Chenjuan Guo, Bin Yang, Qingsong Wen, and Lunting Fan. Noise matters: Cross contrastive learning for flink anomaly detection. *Proc. VLDB Endow.*, 2025.

[Zong *et al.*, 2018] Bo Zong, Qi Song, Martin Renqiang Min, Wei Cheng, Cristian Lumezanu, Daeki Cho, and Haifeng Chen. Deep autoencoding gaussian mixture model for unsupervised anomaly detection. In *International conference on learning representations*, 2018.